

SUBMITTED VERSION

Bo Xu, Shane Waters, Caitlin S. Byrt, Darren Plett, Stephen D. Tyerman, Mark Tester, Rana Munns, Maria Hrmova, Matthew Gilliam

Structural variations in wheat HKT1;5 underpin differences in Na⁺ transport capacity

Cellular and Molecular Life Sciences, 2018; 75(6):1133-1144

© Springer International Publishing AG, part of Springer Nature 2017

This is a pre-print of an article published in Cellular and Molecular Life Sciences. The final authenticated version is available online at: <http://dx.doi.org/10.1007/s00018-017-2716-5>

PERMISSIONS

<https://www.springer.com/gp/open-access/authors-rights/self-archiving-policy/2124>

Publishing in a subscription-based journal

By signing the Copyright Transfer Statement you still retain substantial rights, such as self-archiving:

Author(s) are permitted to self-archive a pre-print and an author's accepted manuscript version of their Article.

a. a pre-print is the author's version of the Article before peer-review has taken place ("Pre-Print"). Prior to acceptance for publication, Author(s) retain the right to make a Pre-Print of their Article available on any of the following: their own personal, self-maintained website; a legally compliant, non-commercial pre-print server such as but not limited to arXiv and bioRxiv. Once the Article has been published, the Author(s) should update the acknowledgement and provide a link to the definitive version on the publisher's website: "This is a pre-print of an article published in [insert journal title]. The final authenticated version is available online at: [https://doi.org/\[insert DOI\]](https://doi.org/[insert DOI])".

12 December 2018

1 Full Title: Structural variations in wheat HKT1;5 underpin
2 differences in Na⁺ transport capacity

3 Running title: Structure-function examination of wheat HKT1;5

4 Authors: Bo Xu^{1,2†}, Shane Waters^{2†}, Caitlin S. Byrt^{1,2}, Darren Plett², Stephen D.
5 Tyerman^{1,2}, Mark Tester³, Rana Munns⁴, Maria Hrmova^{2*} and Matthew Gilliam^{1,2*}

6
7 ¹Australian Research Council Centre of Excellence in Plant Energy Biology,
8 University of Adelaide, Waite Research Precinct, Glen Osmond, South Australia
9 5064, Australia

10
11 ²School of Agriculture, Food and Wine, and Waite Research Institute, University of
12 Adelaide, Waite Research Precinct, Glen Osmond, South Australia 5064, Australia

13
14 ³Center for Desert Agriculture, Division of Biological and Environmental Sciences
15 and Engineering, 4700 King Abdullah University of Science and Technology, Thuwal
16 23955-6900, Kingdom of Saudi Arabia

17
18 ⁴School of Agriculture and Environment, and ARC Centre of Excellence in Plant
19 Energy Biology, University of Western Australia, Crawley 6009, Australia

20
21 †These authors contributed equally

22
23 *Corresponding authors: e-mail: matthew.gilliam@adelaide.edu.au;
24 maria.hrmova@adelaide.edu.au

25
26
27 **Electronic supplementary material**

28 The online version of this article contains supplementary material

29

30 **Abstract**

1
2 31 An important trait associated with the salt tolerance of wheat is the exclusion of
3
4 32 sodium ions (Na^+) from the shoot. We have previously shown that the sodium
5
6 33 transporters TmHKT1;5-A and TaHKT1;5-D, from *Triticum monococcum* (Tm) and
7
8 34 *Triticum aestivum* (Ta), are encoded by genes underlying the major shoot Na^+ -
9
10 35 exclusion loci *Nax1* and *Kn1*, respectively. Here, using heterologous expression we
11
12 36 show that the affinity (K_m) for the Na^+ transport of TmHKT1;5-A, at 2.66 mM, is
13
14 37 higher than that of TaHKT1;5-D at 7.50 mM. Through 3D structural modelling we
15
16 38 identify residues – D⁴⁷¹/a gap and D⁴⁷⁴/G⁴⁷³ that contribute to this property. We
17
18 39 identify four additional mutations in amino acid residues that inhibit the transport
19
20 40 activity of TmHKT1;5-A, which are predicted to be the result of an occlusion of the
21
22 41 pore. We propose that the underlying transport properties of TmHKT1;5-A and
23
24 42 TaHKT1;5-D contribute to their unique ability to improve Na^+ exclusion in wheat that
25
26 43 leads to an improved salinity tolerance in the field.
27
28 44
29
30 45
31
32 46 **Keywords:** gatekeeper cells; salt exclusion; ion transport; structure-function; einkorn;
33
34 47 bread; salt tolerance; *Xenopus*; mutagenesis; yeast; High affinity K^+ Transporter
35
36
37
38
39
40
41
42
43
44
45
46
47
48
49
50
51
52
53
54
55
56
57
58
59
60
61
62
63
64
65

48 **Introduction**

49 The HKT (HIGH AFFINITY (K⁺) POTASSIUM TRANSPORTER) family was
50 named when the first member of this family was identified [1]. The gene encoding
51 this protein was cloned from a cDNA library constructed from K⁺-starved wheat
52 roots, a condition known to induce high affinity K⁺-uptake in plants [1,2]. *HKT1*, now
53 known as *TaHKT2;1*, encodes an integral membrane protein that spans the plasma
54 membrane of the outer cell-types of *Triticum aestivum* (bread wheat) roots [1,3]. As
55 its name suggests, and based on the protein's transport activity when observed in
56 heterologous expression systems, *TaHKT2;1* was proposed to mediate high affinity
57 K⁺ uptake in root cells [1,4]. In both *Xenopus laevis* oocytes and yeast, *TaHKT2;1*
58 functions as a K⁺-Na⁺ symport protein facilitating K⁺ entry when external K⁺ is low,
59 by using an electrochemical gradient for Na⁺ [4]. Na⁺ uniport into heterologous
60 systems and root cells has also been attributed to the *TaHKT2;1* activity, when
61 external Na⁺ concentrations are in the millimolar range [1,5,6]. *TaHKT2;1* expression
62 is also downregulated by high external Na⁺ [7], through a mechanism that has been
63 speculated to limit the entry of Na⁺ into plants, which can be toxic to cells if
64 accumulated to high levels in the cytoplasm – particularly in photosynthetic tissues
65 [8,9].

66
67 More than twenty years after their discovery, it is now clear that HKT proteins are
68 found widely across the plant kingdom, and, are in fact members of the high affinity
69 K⁺/Na⁺ transporting Ktr/TrK/HKT superfamily of proteins present in bacteria (Ktr
70 and TrK), fungi (TrK) and plants (HKT) [10,11]. It has recently been suggested that
71 in bacteria, Ktr transporters could be a part of a larger protein complex that directly
72 interact with a pump-like subunit belonging to the superfamily of P-type ATPases
73 [12]. Based on these observations, the authors proposed a new mechanism that
74 repurposes protein channel architecture for active transport across biomembranes.

75
76 Of the Ktr/TrK/HKT superfamily, HKT proteins are exceptional as some HKTs can
77 facilitate Na⁺ transport without co-transport of K⁺. All Ktr/TrK/HKT proteins are
78 predicted to have eight transmembrane α -helices that fold into 4-fold pseudo-
79 tetramers around a central pore [13-15]. In plants, HKT proteins have been classified
80 into two subfamilies; classes HKT1;x and HKT2;y [3,16], based on the transport
81 characteristics of HKT proteins that were characterised at that stage, and using

1
2
3
4
5
6
7
8
9
10
11
12
13
14
15
16
17
18
19
20
21
22
23
24
25
26
27
28
29
30
31
32
33
34
35
36
37
38
39
40
41
42
43
44
45
46
47
48
49
50
51
52
53
54
55
56
57
58
59
60
61
62
63
64
65

82 sequences predicted to line the entry pore. The class 2 of HKT proteins has thus far
83 only been found in monocots [15,17], and in general these proteins can facilitate K⁺-
84 Na⁺ symport, or at high external concentrations Na⁺-uniport. As also occurs in Ktr
85 and TrK proteins, the selectivity filter lining the entry pore of the class 2 HKT
86 proteins is predicted to be composed of four glycine residues; in TaHKT2;1 these are
87 present at the protein sequence positions 91, 246, 370 and 473. In the class 1 HKT
88 proteins the first glycine within the predicted selectivity filter is substituted with a
89 serine residue [13]. For instance, OsHKT1;5 has a glycine present at the positions
90 264, 391 and 495, and one serine residue at the position 76 [14]. The majority of class
91 1 HKT proteins have no reported K⁺ permeability and function as Na⁺ uniporters
92 only, and this has been linked to the presence of the glycine to serine substitution
93 [3,13-15,18].

94
95 As the HKT family shares a considerable homology and their genetic variation causes
96 a differential transport activity in plants, it is clear that subtle changes in their protein
97 sequences can have a profound influence on transport properties [14,19-23]. Site-
98 directed mutagenesis has been used previously to probe differences in HKT transport
99 properties for TaHKT2;1 [24], DmHKT1 [25], SlHKT1;2 and SpHKT1;2 [26,27],
100 TsHKT1;2 and AtHKT1 [28], making them ideal candidates for detailed structure-
101 function examinations. Three dimensional (3D) models of two OsHKT1;5 proteins
102 were constructed using the crystal structure of a TrkH protein from *Vibrio*
103 *parahaemolyticus* VpTrKH [14,29], and this model was used to predict functional
104 differences between two rice alleles; however, no functional validation of residues
105 responsible for the predicted functional differences was performed [19]. Of the HKT
106 proteins so far characterised in *X. laevis* oocytes, they catalyse Na⁺ transport in a
107 range of affinities (e.g. $K_m = \sim 1-76$ mM for HKT1;x and 0.15 –6.7 mM for HKT2;y)
108 [30-35]. The HKT2;y subfamily members appear to possess a higher Na⁺-uptake
109 affinity than the HKT1;x subfamily; however, HKT1;x proteins are a demonstrated
110 resource for improving salt tolerance in a range of plant species; e.g. AtHKT1;1 in *A.*
111 *thaliana*, OsHKT1;5 from *Oryza sativa* cv. Nona Bokra, TaHKT1;5-D from *T.*
112 *aestivum* and TmHKT1;5-A from *T. monococcum* [19,33,34,36-38]. However, what
113 the structural elements are that result in the differences in transport affinity of these
114 proteins has not yet been determined.

116 We have previously shown that *HKT* genes underpin two major QTL for salt
117 tolerance in wheat; they both encode proteins that reside on the plasma membrane of
118 cells that surround the vasculature and withdraw Na⁺ from the transpiration stream
119 preventing it from reaching the shoot where it can do damage to photosynthetic
120 apparatus [33,34,39,40]. Hexaploid bread wheat, *T. aestivum* has three genomes; it is
121 the D genome carrying *TaHKT1;5-D* within the *Kna1* locus that confers the Na⁺-
122 excluding ability so important to the greater salt tolerance of bread wheat [41]. An
123 ancestral diploid wheat relative, *Triticum monococcum* (einkorn wheat), carries the
124 homologue *TaHKT1;5-A* on the A genome. *T. monococcum* is not a progenitor to
125 modern wheat and was the source of the *Nax2* QTL [41]. This represents an additional
126 source of Na⁺ exclusion that was shown to produce an increase in yield of 25% in
127 saline soil when introgressed into the tetraploid durum wheat that lacks any
128 homologues of this gene [33].

129
130 In the current work we construct new 3D models for for HKT proteins by using a
131 more recently solved crystal structure of the KtrB K⁺ transporter from *Bacillus*
132 *subtilis* [14,15,42]. We then use this model to determine the impact of particular
133 amino acid residues on the function of TmHKT1;5-A and TaHKT1;5-D. The model
134 indicates why several mutations abolish the function of TmHKT1;5-A and predicts
135 the residues that result in different Na⁺-transport affinities between TmHKT1;5-A and
136 TaHKT1;5-D. The impact of mutations and residue substitutions of interest were
137 confirmed through site-directed mutagenesis and functional characterization of these
138 HKT proteins in *X. laevis oocytes*.

139 **Results**

140 **G490R and K118E/L339P/Y379M mutations abolished the transport properties** 141 **of TmHKT1;5-A**

142 Munns et al. [33] functionally characterised the gene product of *TmHKT1;5-A*, which
143 was previously proposed by Byrt et al. [41] as the candidate gene underlying the shoot
144 Na⁺ exclusion QTL *Nax2*. At this time, two other *TmHKT1;5-A* variants were isolated
145 but not reported. In one of the *TmHKT1;5-A* variants, four nucleotides differed from
146 the *TmHKT1;5-A* sequence lodged with NCBI (DQ646332, [33]). These variations
147 resulted in three amino acid residue changes in TmHKT1;5-A^{K118E/L339P/Y379M} (Fig.
148 S1). A single nucleotide variation was found in an additional variant, which yielded a
149

150 single amino acid residue difference in the protein sequence of TmHKT1;5-A^{G490R}
151 (Fig. S1). These two variants were isolated from plasmid DNA in which the gene had
152 been inserted after it had been cloned from *T. turgidum* Line 149 and had then
153 undergone replication in *E. coli*. The *TmHKT1;5-A* sequence without mutations
154 (DQ646339) was amplified directly from cDNA synthesised from RNA isolated from
155 Line 149 by Polymerase Chain Reaction (PCR). The variants identified here are
156 unlikely to be naturally occurring in wheat as they differ in sequence from the three
157 *HKT1;5* in *T. turgidum*, which are all present on the B genome only (DQ646333,
158 DQ646334, DQ646335); B genome members of *HKT1;5* also have very low
159 expression [32]. Furthermore, the A genome version of *HKT1;5* is derived from a
160 cross with *T. monococcum* – with Line 149 fixed for this allele – so it cannot be the
161 source of three different versions of the same gene. Instead, it is likely that the Single
162 Nucleotide Polymorphism (SNP) changes identified in these variants originated from
163 the spontaneous mutation of *TmHKT1;5-A* in *E. coli*. Although there is no evidence to
164 suggest that either of two variants naturally occur in wheat, these variants provided an
165 opportunity to investigate how variation in protein sequences may alter HKT transport
166 properties.

167
168 We were particularly interested in the properties of TmHKT1;5-A^{G490R}. Gly is a
169 neutral residue and the Gly490 residue is highly-conserved across most plant
170 HKT1;5-like proteins that have been characterised or identified. The exception to this
171 is EchKT1;1 (also known as EchKT1) from *Eucalyptus camaldulensis* that instead
172 has the polar amino acid residue Ser (Fig. 1a and Fig. S2) [15,43,44]; the crystallised
173 K⁺ transporter, VpTrkH has a hydrophobic Ala residue in this position [29] (Fig. S2).
174 The residues associated with the other TmHKT1;5-A variant were not conserved: the
175 K118 position was occupied by a variety of residues in 84% of the sequences
176 analysed, including Glu, whilst the L339 position was substituted by hydrophobic
177 Met, Leu, Val, Ala, Phe, Ile or hydrophilic Thr, but never by a Pro, and the Y379
178 position was occupied in 92% of the analysed sequences by other polar residues or by
179 hydrophobic Pro, Leu and Val, but never Met (Table S2).

180
181 The growth of yeast transformed with either of the two *TmHKT1;5-A* variants
182 (TmHKT1;5-A^{K118E/L339P/Y379M} or TmHKT1;5-A^{G490R}) was indistinguishable from the
183 growth of the vector-control-containing yeast on SC-Ura plates with 10 or 200 mM

184 Na⁺ (Fig. 1b). Yeast containing *AtHKT1;1*, a positive HKT control, known to
185 transport Na⁺ and induce a growth reduction in yeast in high salt [18] grew on media
186 containing 10 mM Na⁺ but not 200 mM Na⁺ (Fig. 1b). However, growth of yeast
187 transformed with *TmHKT1;5-A* was suppressed when grown on 10 mM Na⁺ (Fig. 1b)
188 [33]. In an arginine-phosphate (AP)-based medium with low Na⁺ (< 8 μM) and K⁺ (<
189 5 μM) [45], the growth of yeast expressing *TmHKT1;5-A* was similar to that of vector
190 control and two *TmHKT1;5-A* variants (Fig. 1c). In the AP liquid medium with 10
191 mM NaCl (equivalent to the amount of Na⁺ in the SC-Ura agar medium) the growth
192 of yeast containing *TmHKT1;5-A* was suppressed compared with that of the empty-
193 vector control and the two variants.

194
195 To understand the Na⁺ transport properties of TmHKT1;5-A and the two variants
196 TmHKT1;5-A^{K118E/L339P/Y379M} and TmHKT1;5-A^{G490R}, we analysed the currents
197 associated with expressing these proteins in *X. laevis* oocytes. First, we confirmed
198 through confocal imaging that YFP-TmHKT1;5-A chimeric proteins were localised to
199 the plasma membrane of oocytes (Fig. 1d). Previously, we demonstrated that oocytes
200 injected with TmHKT1;5-A-cRNA elicited significant inward currents in the presence
201 of Na⁺ [33] and here we show they accumulated 140% higher Na⁺ and 40% lower K⁺
202 than control oocytes (Fig. 1e). Oocytes injected with either variant had similar ion
203 contents to water-injected controls (Fig. 1e), also both variant-cRNA-injected oocytes
204 produced currents that were insignificantly different to control oocytes (water-
205 injected), that mediated little Na⁺- or K⁺-dependent inward currents (Fig. 1f, g). In
206 comparison, oocytes expressing *TmHKT1;5-A* produced a large Na⁺-dependent
207 current which was not induced by K⁺ (Fig. 1f, g). Both the data from yeast and
208 oocytes indicated that neither of the TmHKT1;5-A variants carried any significant
209 Na⁺ currents and so were likely to be rendered non-functional by their mutations.

210 211 **3D structural modelling of TaHKT1;5-D and TmHKT1;5-A**

212 We constructed 3D models to investigate whether we could determine a structural
213 basis for the functional observations made above (Fig. 2-3 and Fig. S3). These models
214 were based on spatial restraints that reflect a structural similarity between the plant
215 HKT class of proteins and the KtrB K⁺ transporter from *B. subtilis* [42]. At least 100
216 models were constructed from each alignment and assessed by the Discrete Optimized
217 Protein Energy (DOPE) scoring function [3], PROCHECK [46] and ProSa2003 [47].

1 218 The most favourable models were constructed on the basis of AA2 alignments [48],
2 219 using the MUSCLE algorithm [49]. However the first 26 amino acid residues of
3 220 TaHKT1;5-D and TmHKT1;5-A were deleted from the protein sequences before
4 221 running Modeller as this section had no structural counterpart in the KtrB template. A
5 222 Ramachandran plot of the KtrB template (4J7C:I), TaHKT1;5-D, TmHKT1;5-A, and
6 223 the G490R and K118E/L339P/Y379M variants with PROCHECK indicated that
7 224 100% (429), 99.5% (429), 99.3% (431), 98.4% (428) and 99.5% (431) residues were
8 225 in the most favoured, additionally allowed and generously allowed regions, when
9 226 excluding Gly and Pro residues. The overall G-factors (estimates of stereo-chemical
10 227 parameters by PROCHECK) were 0.08, -0.21, -0.19, -0.14 and -0.20, and the
11 228 ProSa2003 z-scores were -8.5, -6.1, -6.1, -6.2 and -6.0 for 4J7C:I, TaHKT1;5-D,
12 229 TmHKT1;5-A, G490R and K118E/L339P/Y379M, respectively. DOPE analyses [50]
13 230 did not reveal any substantial deviations from the global energy profiles. To assess the
14 231 level of conservation of individual amino acid residues, the TaHKT1;5-D model was
15 232 analysed through the ConSurf server [51,52], using 234 sequences at 35%-95%
16 233 sequence identity to TaHKT1;5-D (Table S2).

17 234
18 235 The final 3D models of TaHKT1;5-D and TmHKT1;5-A (Fig. S3a and S3b)
19 236 highlighted the overall architectures of both transporters with the well-defined Ser-
20 237 Gly-Gly-Gly motifs (S78, G233, G353, G457) [14,15] that form the body of the
21 238 selectivity filter at its narrowest point (*cf.* black arrows in Fig. S3). These motifs are
22 239 consistent with these proteins being highly selective for Na⁺ over K⁺, as opposed to
23 240 the Gly-Gly-Gly-Gly motif seen in less-selective Na⁺/K⁺ HKT proteins [3], or in the
24 241 bacterial superfamily K⁺ transporters TrkH [29] and KtrB [42].

242 243 **Structural modifications in the TmHKT1;5-A variants**

244 We used the models to investigate whether there were any obvious structural changes
245 that may explain the lack of function of the two TmHKT1;5-A variants (Fig. 2).
246 Compared to the wild-type protein (Fig. 2a), the change in the Van der Waals volume
247 of TmHKT1;5-A^{G490R} (Fig. 2b) indicates that the Arg side chain formed by the
248 G490R substitution is likely to project into the pore, resulting in less space for ions to
249 move through the pore. For TmHKT1;5-A^{K118E/L339P/Y379M}, the L339P substitution
250 locates to a loop adjoining two α -helices (Fig. 2c), and may lead to the loss of
251 structural flexibility in this particular part of the protein. The K118E substitution is

1
2
3
4
5
6
7
8
9
10
11
12
13
14
15
16
17
18
19
20
21
22
23
24
25
26
27
28
29
30
31
32
33
34
35
36
37
38
39
40
41
42
43
44
45
46
47
48
49
50
51
52
53
54
55
56
57
58
59
60
61
62
63
64
65

252 also positioned on a loop, but is located in the proximity of two short neighbouring α -
253 helices that may be affected by the negative charge of original Glu. This non-
254 conservative substitution from basic Lys to acidic Glu could have a significant impact
255 on the stability of this part of the structure. The third substitution Y379M takes place
256 within the protein cavity that opens from the distal part of the selectivity filter, and is
257 positioned on a short loop linking two α -helices that form the outer scaffold of the
258 protein. While this substitution is not likely to directly affect the passage of ions
259 through the pore, we still consider it to be significant for the integrity of the protein
260 structure. The presence of the aromatic moiety of Tyr at the interface of two α -helices
261 could be important for close packing and co-ordination of the dynamics of the
262 neighbouring α -helices, and thus this Y379M substitution could destabilise this inter-
263 α -helical interactions. We did not probe these mutations further as they make the
264 protein non-functional, instead we explored whether we could use the molecular
265 model we constructed to examine whether we could improve the transport function of
266 the HKT proteins.

267

268 **The structural basis of TaHKT1;5-D and TmHKT1;5-A Na⁺ transport affinity**

269 The TmHKT1;5-A and TaHKT1;5-D proteins share 95% positional sequence
270 identity; they are 517 and 516 amino acid residues in length, respectively, with 27
271 residue differences between them (Table S1; Fig. S4). However, TmHKT1;5-A has
272 been
273 reported to have a lower K_m for Na⁺ transport than TaHKT1;5-D [33,34]. The
274 comparisons of the structural models for TmHKT1;5-A and TaHKT1;5-D allowed us
275 to predict the residues that most likely contribute to structural differences between the
276 two proteins, and therefore are likely to underlie the differences in transport affinity
277 (Fig. 3). Six amino acid residue substitutions, which are likely to have significant
278 structural implications have been summarized in Table 1, and are also displayed in
279 Figs. 3 and S4. When superimposed, the respective D⁴⁷¹/a gap (or a deletion) and
280 D⁴⁷⁴/G⁴⁷³ motifs, in TmHKT1;5-A or TaHKT1;5-D were deemed as candidates likely
281 to have the most profound impact on HKT structures and thus affect transport rates.
282 Interestingly, the D471 position in TmHKT1;5-A was altered only in 15% sequences
283 to mostly polar residues, such as Ser, Asp, Glu and Lys, but also to hydrophobic Ala
284 and Pro, while the D474 position was highly variable and in 87% sequences was
285 occupied by other 19 residues (Table S2).

1
2
3
4
5
6
7
8
9
10
11
12
13
14
15
16
17
18
19
20
21
22
23
24
25
26
27
28
29
30
31
32
33
34
35
36
37
38
39
40
41
42
43
44
45
46
47
48
49
50
51
52
53
54
55
56
57
58
59
60
61
62
63
64
65

286 **D⁴⁷¹/a gap and D⁴⁷⁴/G⁴⁷³ differentiate the Na⁺ transport affinity of TmHKT1;5-A**
287 **and TaHKT1;5-D**

288 We further examined D⁴⁷¹/a gap and D⁴⁷⁴/G⁴⁷³ using site-directed mutagenesis to
289 explore whether these mutations affected the Na⁺ transport activity of TmHKT1;5-A
290 and TaHKT1;5-D. Initially to confirm the differential Na⁺ transport activity of
291 TmHKT1;5-A and TaHKT1;5-D [31,32] we expressed each gene in *X. laevis* oocytes
292 and found that the Na⁺ transport affinity of TmHKT1;5-A was significantly higher
293 than of TaHKT1;5-D, by three-fold ($K_m = 2.66 \pm 0.35$ vs. 7.5 ± 1.24 mM; $P=0.0028$,
294 Students t-test) (Fig. 4-5). Therefore, we performed a mutagenesis by PCR to delete
295 D⁴⁷¹ (TmHKT1;5-A^{D471Δ}), mutate D⁴⁷⁴ into G (TmHKT1;5-A^{D474G}) or delete/mutate
296 both residues (TmHKT1;5-A^{D471Δ/D474G}). In addition, TaHKT1;5-D was mutated with
297 an insertion of D⁴⁷¹ (TaHKT1;5-D^{D471+}), a mutation of G⁴⁷³ into D (TaHKT1;5-
298 D^{G473D}) and a double mutation (TaHKT1;5-D^{D471+/G473D}). When expressed in *X. laevis*
299 oocytes and irrigated with a 5 mM Na⁺ solution, the oocytes containing the double
300 mutation D471Δ/D474G in TaHKT1;5-A showed a significant reduction in the Na⁺
301 conductance from 46.19 ± 13.25 μS (of TmHKT1;5-A) to 18.22 ± 2.65 μS (of
302 TmHKT1;5-A^{D471Δ/D474G}) (Fig. 4a, b). These double mutations also led to a significant
303 decrease in the Na⁺ transport affinity of this variant from $K_m = 2.66 \pm 0.35$ mM of
304 wild-type TmHKT1;5-A to 4.10 ± 0.42 mM (Fig. 4a,c). The single mutation of either
305 D471Δ or D474G increased K_m values (respective values are 3.28 ± 0.53 mM and
306 4.62 ± 1.29 mM), but these were statistically insignificant (Fig. 4c).

307
308 The reciprocal mutations were performed on TaHKT1;5-D. The single mutation
309 G473D and double mutation D471⁺/G473D significantly increased the conductance of
310 TaHKT1;5-D from 25.54 ± 5.78 μS to 66.2 ± 8.49 μS and 69.35 ± 9.58 μS in 5 mM
311 Na⁺ solution respectively (Fig. 5a, b). Again, only the double mutation significantly
312 changed its transport affinity ($K_m = 3.93 \pm 0.57$ mM), with the single mutations –
313 D471⁺ and G473D leading to insignificant changes in the Na⁺ transport affinity of
314 TaHKT1;5-D, to $K_m = 4.48 \pm 1.2$ mM and 5.01 ± 0.77 mM, respectively (Fig. 5c).

315
316 **Discussion**

317 Crystal structures of the potassium ion transporters TrkH protein from *Vibrio*
318 *parahaemolyticus* and KtrB from *B. subtilis* have been solved [29,42]. These

1
2
3
4
5
6
7
8
9
10
11
12
13
14
15
16
17
18
19
20
21
22
23
24
25
26
27
28
29
30
31
32
33
34
35
36
37
38
39
40
41
42
43
44
45
46
47
48
49
50
51
52
53
54
55
56
57
58
59
60
61
62
63
64
65

319 bacterial proteins together with plant HKT proteins are all part of the same
320 superfamily of K⁺ transporters [15]. However, the KtrB template has a better
321 sequence similarity to the HKT1;5 class of proteins than that of the TrkH K⁺
322 transporter previously used to model rice HKT1;5 proteins [14] and HKT proteins in
323 wheat [23]. Compared to the previous model the positioning of loops connecting the
324 α -helices and the C-terminal ends of the proteins had an improved structural
325 similarity, although this was still only at 23% sequence identity. However, the α -
326 helical bundle component of the TaHKT1;5-D and TmHKT1;5-A proteins aligned
327 well with the KtrB template indicating a reliable modelling of their structure and
328 therefore the model we propose here is an advance; a crystal structure of a HKT
329 would obviously lend a better model, but until that occurs this is the best structural
330 model for wheat HKT1;5 class proteins currently available. Therefore, we used this
331 new HKT model to investigate the structural and functional differences between
332 HKT1;5 proteins.

333
334 Our functional studies indicated that two variants TmHKT1;5-A^{G490R} and
335 TmHKT1;5-A^{K118E/L339P/Y379M}, were non-functional. Despite the protein being
336 localised in the plasma membrane, no Na⁺ currents were detected when expressed in
337 *X. laevis* oocytes and no Na⁺-induced growth inhibition of *S. cerevisiae* was apparent
338 unlike in yeast expressing *TmHKT1;5-A* (Fig. 1). In Fig. 1a and Fig. S2, it can be
339 seen that the Gly490 residue is highly conserved in other HKT1;5-A-like proteins,
340 suggesting that it is an important residue for transport function or for structural
341 integrity. Our structural analysis indicated that the TmHKT1;5-A^{G490R} substitution
342 occurred in a side chain that carries a positive charge at physiological pH. This
343 combined with its likely steric hindrance obstructing the pore, would present a barrier
344 to cations moving through the extension of the selectivity filter (Fig. 2 and Fig. S3).
345 Furthermore, this mutation may affect the pore rigidity and dispositions of
346 neighbouring residues controlling the rates of Na⁺ transport. Therefore, in summary,
347 the structural penalties caused by the G490R variation may work in concert and
348 explain the loss of Na⁺ transport activity by this variant of the TmHKT1;5-A protein.
349 For, TmHKT1;5-A^{K118E/L339P/Y379M}, all the amino acid residue substitutions are non-
350 conservative (Table S2). Y379 was found to be the least conserved of the three, this
351 position was usually occupied by an aromatic residue with Ser being a common
352 exception. The K118E and Y379M substitutions were only observed in 1% of the

1
2
3
4
5
6
7
8
9
10
11
12
13
14
15
16
17
18
19
20
21
22
23
24
25
26
27
28
29
30
31
32
33
34
35
36
37
38
39
40
41
42
43
44
45
46
47
48
49
50
51
52
53
54
55
56
57
58
59
60
61
62
63
64
65

353 sequences, while the L339P substitution remained undetected. As described in the
354 results, we propose that these three substitutions largely destabilise the TmHKT1;5-A
355 structure and result in a loss of function.

356
357 Using our molecular models, we turned our attention to making predictions regarding
358 the residue differences that are likely to contribute to the higher affinity of Na⁺
359 transport observed for TmHKT1;5-A compared to TaHKT1;5-D (Fig. 4 and 5). There
360 are 27 amino acid residue differences between these two proteins, and through our
361 analysis we predicted that six residue substitutions were likely to be significant (Table
362 1 and Fig. 3). Of these six, there were two residues, D471 and D474 from
363 TmHKT1;5-A that were particularly interesting because this combined pair of
364 aspartic acids at these sites were not observed in any of 48 other HKT members
365 analysed, except OsHKT2;4 which has an aspartic acid at the site 466 but an alanine
366 at site 469 (Fig. S5). Indeed, the D471/a gap and D474/473G substitutions occur very
367 close to each other and form a part of an α -helix which directly links to one of the
368 loops forming the selectivity filter. Double mutations of these two residues –
369 D471 Δ /D473G and D471⁺/G473D, respectively, – caused a reduction in the
370 TmHKT1;5-A Na⁺ transport affinity while increasing it for TaHKT1;5-D. This
371 resulted in the Na⁺ transport affinity of TmHKT1;5-A^{D471 Δ /D474G} ($K_m = \sim 3.9$ mM) and
372 TaHKT1;5-D^{D471⁺/G473D} ($K_m = 4.1$ mM) to be at a similar level. Nevertheless,
373 TmHKT1;5-A^{D471 Δ /D474G} still had a higher Na⁺ transport affinity than wild-type
374 TaHKT1;5-D ($P = 0.0076$), suggesting that other substitutions listed in Table S1 are
375 likely to further contribute to the observed functional differences. The D471 Δ /D473G
376 substitutions decreased the transport conductance of TmHKT1;5-A^{D471 Δ /D474G}, close
377 to that of TaHKT1;5-D ($P = 0.6439$); while TaHKT1;5-D^{D471⁺/G473D} had a comparable
378 conductance to TmHKT1;5-A ($P = 0.5136$) (Fig. 4a, b). So these two motifs (D471/a
379 gap and G473/474D) have a key influence on the Na⁺-uptake capacity of TmHKT1;5-
380 A/TaHKT1;5-D. We did not find evidence that these mutations are naturally
381 occurring within wheat, but these could be investigated in the future through the use
382 of molecular markers on wheat diversity panels. An extension of the model to include
383 other HKT proteins, a greater survey of structure-function relationships and
384 experimental mutations of key residues both *in vitro* and *in vivo* to explore the wider
385 functional significance of these differences will be the focus of a further study.

386

1
2
3
4
5
6
7
8
9
10
11
12
13
14
15
16
17
18
19
20
21
22
23
24
25
26
27
28
29
30
31
32
33
34
35
36
37
38
39
40
41
42
43
44
45
46
47
48
49
50
51
52
53
54
55
56
57
58
59
60
61
62
63
64
65

387 TmHKT1;5-A facilitates Na⁺ uptake with a higher affinity than TaHKT1;5-D (Fig. 4-
388 5). We studied the K_m of these proteins, as this is the parameter in which we could
389 have most confidence. Whereas V_{max} may be susceptible to misinterpretation due to
390 potential differences in protein expression between *X. laevis* oocytes, K_m values will
391 not. Importantly, physiologically relevant concentrations in the stele (i.e. in the low
392 mM range; Table III [8]), coincide with the K_m of TmHKT1;5-A. This suggests that
393 the higher mM values for the K_m of TaHKT1;5-D would render it less effective in
394 retrieving Na⁺ into stelar cells and therefore is a potential explanation of how it
395 confers less Na⁺ exclusion. Consistent with this proposition, the introgression of the
396 *Nax2* locus carrying *TmHKT1;5-A* into bread wheat confers greater Na⁺-exclusion to
397 bread wheat which already carries *TaHKT1;5-D* [53].

398
399 The expression of class 1 *HKT* genes can elicit downstream responses that lead to an
400 increased exclusion of Na⁺ from the shoot [33,34,37,38]. We envisage that HKT1;5-
401 like proteins may stimulate retrieval of Na⁺ from the stelar apoplast, specifically from
402 the xylem vessel elements, and effectively act as a node setting off a cascade of
403 downstream processes that lead to greater plant salt tolerance. These processes
404 involve the increased activity of proteins involved in compartmentation of Na⁺ within
405 the root vacuoles of specific cell-types and the cortex [9,37,38] and potentially those
406 that catalyse the efflux of Na⁺ from roots. Stelar cells, and in particular those cells that
407 line the xylem, clearly play an important role in limiting the salt transport to the shoot
408 and in conferring plant salt tolerance. As such, we consider it instructive to think of
409 this action as constituting a ‘gatekeeper’ process. *i.e.* a discrete cell-type that provides
410 a rate limiting step for the control the flux of solutes into or throughout the plant, be
411 they nutrients, toxins or metabolites. We consider that it is imperative that the unique
412 transport processes within populations of these gatekeeper cell-types are further
413 studied to understand how the net flux of solutes through plant tissues occurs [54].

414
415 Coupling previous research [33,34] with the comparison of two Na⁺-selective
416 channels in this study suggests that the candidate gene *TmHKT1;5-A* in the *Nax2*
417 locus from ancestral wheat germplasm *T. monococcum* encodes a unique high affinity
418 Na⁺-exclusion transporter. We propose that this locus serves as an optimal choice for
419 wheat breeders for developing salinity tolerant wheat lines with more efficient Na⁺-
420 exclusion.

421

422 **Materials and Methods**

423 Brief methods for cloning of *TmHKT1;5-A* and variants as well as its functional
424 characterisation in heterologous expression systems of *X. laevis* oocyte and
425 *Saccharomyces cerevisiae* were described Munns et al. [33] and Byrt et al. [34].
426 More detailed methods for protein modelling were included in Cotsaftis et al. [14].
427 Further details are included here.

428

429 **Gene cloning and site-directed mutagenesis**

430 *TmHKT1;5-A* was isolated from both cDNA of durum wheat (*T. turgidum*) Line 149
431 roots and the *T. monococcum* (DV92) BAC library [33,34,41,55]. The following site-
432 directed-mediated mutagenesis PCR was performed on these entry clones as
433 templates to create single or double mutations of *TmHKT1;5-A* and *TaHKT1;5-D* as
434 indicated in a Figure legend, using the Phusion™ Hot Start High-Fidelity DNA
435 polymerase (FINNZYMES) with primers as listed in Table S3. PCR products were
436 purified from agarose gel and phosphorylated by the T4 Polynucleotide Kinase
437 (New England Biolabs) to add a phosphate group to the 5' and 3' ends of the products
438 at 37 °C for 30 min. These were subsequently self-ligated by the T4 DNA Ligase
439 (New England Biolabs) at 4 °C overnight. Ligase reactions were transformed into
440 TOP10 Chemically Competent *E. coli* cells (Invitrogen).

441

442 **Plasmid construction**

443 The vector containing a YFP tag for heterologous expression in *X. laevis* oocytes was
444 constructed using a restriction digest and ligation of two expression vector fragments.
445 The pGEMHE-DEST vector for *X. laevis* oocyte expression was cut by *SmaI* and
446 *XbaI* to remove the Gateway cloning site and to provide a backbone; then the same
447 enzyme set was used to cut the Gateway cloning cassette with *YFP* tagged on the N-
448 terminus from pBS-YFP-attR. Two fragments were fused together into a new
449 expression vector named pYFP-GEMHE using the T4 ligase (New England Biolabs).
450 *TmHKT1;5-A*^{K118E/L339P/Y379M} and *TmHKT1;5-A*^{G490R} were recombined from the entry
451 vector into the new pYFP-GEMHE using Gateway LR Clonase II Enzyme mix
452 (Invitrogen).

453

1
2
3
4
5
6
7
8
9
10
11
12
13
14
15
16
17
18
19
20
21
22
23
24
25
26
27
28
29
30
31
32
33
34
35
36
37
38
39
40
41
42
43
44
45
46
47
48
49
50
51
52
53
54
55
56
57
58
59
60
61
62
63
64
65

454 **Fluorescence imaging of TmHKT1;5-A variant to investigate membrane**

455 **localisation in *X. laevis* oocytes**

456 The recombinant expression vector pYFP-GEMHE carrying *TmHKT1;5-*
457 *A*^{K118E/L339P/Y379M} or *TmHKT1;5-A*^{G490R} was linearised by *SbfI* (New England Biolabs).
458 cRNA was synthesised from linearised plasmid using the mMMESSAGE mMACHINE
459 T7 Transcription Kit, following manufacturer's instructions (Ambion). 46 nl/46 ng of
460 cRNA was injected into oocytes with a Nanoinject II microinjector (Drummond
461 Scientific). Oocytes were incubated for 48 h at 18 °C before imaging using a confocal
462 laser scanning microscope equipped with a Zeiss Axioskop 2, LSM5 PASCAL and
463 an argon laser (Carl Zeiss). Sequential scanning and laser excitation was used to
464 capture fluorescence from YFP (excitation = 514 nm, emission band pass = 570–590
465 nm).

466
467 **Two-electrode voltage clamp recording in *X. laevis* oocytes**

468 Oocyte recording followed the methods as described in Munns et al. [33] and Byrt et
469 al. [34]. Briefly, 46 nl/23 ng of cRNA or equal volumes of RNA-free water were
470 injected into oocytes, followed by an incubation for 48 h before recording. Membrane
471 currents were recorded in the HMg solution (6 mM MgCl₂, 1.8 mM CaCl₂, 10 mM
472 MES and pH 6.5 adjusted with a TRIS base) ± Na⁺ glutamate and/or K⁺ glutamate as
473 indicated. All solution osmolarities were adjusted using mannitol at 220-240 mOsmol
474 kg⁻¹.

475
476 **Construction of 3D models of TaHKT1;5-D, TmHKT1;5-A and the G490R and**
477 **K118E/L339P/Y379M variants of TmHKT1;5-A**

478 The most suitable template for TaHKT1;5-D, TmHKT1;5-A and variants of
479 TmHKT1;5-A, identified by Phyre2 [56] and I-TASSER [57], was the KtrB K⁺
480 transporter from *B. subtilis* (Protein Data Bank accession 4J7C, chain I referred to as
481 4J7C:I) [42]. This template replaces the TrkH K⁺ transporter (Protein Data Bank
482 accession 3PJZ, chain K referred to as 3PJZ:K) [29] that was previously used to
483 model rice HKT proteins [14]. The KtrB K⁺ structure was crystallised in the presence
484 of 150 mM KCl and contains a K⁺ ion in the central pore. This ion was substituted by
485 Na⁺ ion during modelling of wheat HKT proteins because TaHKT1;5-D and
486 TmHKT1;5-A proteins transport Na⁺ and not K⁺. As the respective sequence identity
487 and similarity between TmHKT1;5-A and 4J7C:I (23% and 59%), and TaHKT1;5-D
and 4J7C:I (23% and 61%) were low a variety of alignments obtained through

1
2
3
4
5
6
7
8
9
10
11
12
13
14
15
16
17
18
19
20
21
22
23
24
25
26
27
28
29
30
31
32
33
34
35
36
37
38
39
40
41
42
43
44
45
46
47
48
49
50
51
52
53
54
55
56
57
58
59
60
61
62
63
64
65

488 LOMETS [58], PROMALS3D [59], MUSCLE [49] and AA2 [48] were applied to
489 generate models in complex with Na⁺, using Modeller 9v8 [60] on a Linux station
490 running the Fedora 12 operating system.

491

492 **Statistical analysis**

493 All analysis and graphing was performed in Graphpad Prism version 7. Statistical tests
494 were performed as stated in the text or figure legends.

495

496 **Funding**

497 This work was supported by the Grains Research and Development Corporation
498 (UA00145, M.G.), the University of Adelaide Australian Postgraduate Award and the
499 CJ Everald postgraduate scholarship (S.W.), and the Australian Research Council
500 through the following schemes: Discovery (DP120100900, M.H.), Centre of
501 Excellence (CE140100008, M.G., R.M., S.D.T), Future Fellowship (FT130100709,
502 M.G.), and DECRA (DE150100837, C.S.B.).

503

504 **Author contribution**

505 B.X., M.H., D.P. and M.G. conceived the project out of work initiated by R.M. and
506 M.T.. B.X. performed all experiments except the structural modelling and predictions
507 (S.W.) and the cloning and original characterisation of TmHKT1;5-A^{K118E/L339P/Y379M}
508 (C.S.B.). S.D.T. advised on electrophysiology and analysis. M.G, M.H. and D.P.
509 supervised the work. B.X., S.W., C.S.B., M.H. and M.G. wrote the paper. All authors
510 provided comment.

511

512 **Acknowledgements**

513 N/A

514

515 **References**

- 516 1. Schachtman DP, Schroeder JI (1994) Structure and transport mechanism of a high-
517 affinity potassium uptake transporter from higher plants. *Nature* 370:655-658
- 518 2. Epstein E (1966) Dual pattern of ion absorption by plant cells and by plants. *Nature*
519 212:1324-1327
- 520 3. Platten JD, Cotsaftis O, Berthomieu P, Bohnert H, Davenport RJ, Fairbairn DJ,
521 Horie T, Leigh RA, Lin H-X, Luan S (2006) Nomenclature for HKT transporters,
522 key determinants of plant salinity tolerance. *Trends Plant Sci* 11 (8):372-374

- 523 4. Rubio F, Gassmann W, Schroeder JI (1995) Sodium-driven potassium uptake by
524 the plant potassium transporter HKT1 and mutations conferring salt tolerance.
525 Science 270 (5242):1660-1663
- 526 5. Gierth M, Mäser P (2007) Potassium transporters in plants—involvement in K⁺
527 acquisition, redistribution and homeostasis. FEBS Lett 581 (12):2348-2356
- 528 6. Horie T, Hauser F, Schroeder JI (2009) HKT transporter-mediated salinity
529 resistance mechanisms in *Arabidopsis* and monocot crop plants. Trends Plant Sci
530 14 (12):660-668
- 531 7. Laurie S, Feeney KA, Maathuis FJ, Heard PJ, Brown SJ, Leigh RA (2002) A role
532 for HKT1 in sodium uptake by wheat roots. Plant J 32 (2):139-149
- 533 8. James RA, Davenport RJ, Munns R (2006) Physiological characterization of two
534 genes for Na⁺ exclusion in durum wheat, *Nax1* and *Nax2*. Plant Physiol 142
535 (4):1537-1547
- 536 9. Läuchli A, James RA, Huang CX, McCluy M, Munns R (2008) Cell-specific
537 localization of Na⁺ in roots of durum wheat and possible control points for salt
538 exclusion. Plant Cell Environ 31 (11):1565-1574
- 539 10. Sentenac H, Bonneaud N (1992) Cloning and expression in yeast of a plant
540 potassium ion transport system. Science 256 (5057):663-665
- 541 11. Corratgé-Faillie C, Jabnour M, Zimmermann S, Véry A-A, Fizames C, Sentenac
542 H (2010) Potassium and sodium transport in non-animal cells: the Trk/Ktr/HKT
543 transporter family. Cell Mol Life Sci 67 (15):2511-2532
- 544 12. Huang CS, Pedersen BP, Stokes DL (2017) Crystal structure of the potassium-
545 importing KdpFABC membrane complex. Nature 546 (7660):681-685
- 546 13. Mäser P, Hosoo Y, Goshima S, Horie T, Eckelman B, Yamada K, Yoshida K,
547 Bakker EP, Shinmyo A, Oiki S (2002) Glycine residues in potassium channel-like
548 selectivity filters determine potassium selectivity in four-loop-per-subunit HKT
549 transporters from plants. Proc Natl Acad Sci USA 99 (9):6428-6433
- 550 14. Cotsaftis O, Plett D, Shirley N, Tester M, Hrmova M (2012) A two-staged model
551 of Na⁺ exclusion in rice explained by 3D modeling of HKT transporters and
552 alternative splicing. PLoS One 7 (7):e39865
- 553 15. Waters S, Gilliam M, Hrmova M (2013) Plant high-affinity potassium (HKT)
554 transporters involved in salinity tolerance: structural insights to probe differences
555 in ion selectivity. Int J Mol Sci 14 (4):7660-7680
- 556 16. Singh A, Bhushan B, Gaikwad K, Yadav OP, Kumar S, Rai RD (2015) Induced
557 defence responses of contrasting bread wheat genotypes under differential salt
558 stress imposition. Indian J Biochem Biophys 52 (1):75-85
- 559 17. Asins MJ, Villalta I, Aly MM, Olias R, Álvarez De Morales P, Huertas R, Li J,
560 Jaime-Pérez N, Haro R, Raga V (2013) Two closely linked tomato HKT coding
561 genes are positional candidates for the major tomato QTL involved in Na⁺/K⁺
562 homeostasis. Plant Cell Environ 36 (6):1171-1191
- 563 18. Uozumi N, Kim EJ, Rubio F, Yamaguchi T, Muto S, Tsuboi A, Bakker EP,
564 Nakamura T, Schroeder JI (2000) The *Arabidopsis* HKT1 gene homolog mediates
565 inward Na⁺ currents in *Xenopus laevis* oocytes and Na⁺ uptake in *Saccharomyces*
566 *cerevisiae*. Plant Physiol 122 (4):1249-1260
- 567 19. Ren ZH, Gao JP, Li LG, Cai XL, Huang W, Chao DY, Zhu MZ, Wang ZY, Luan
568 S, Lin HX (2005) A rice quantitative trait locus for salt tolerance encodes a
569 sodium transporter. Nat Genet 37 (10):1141-1146
- 570 20. Negrão S, Cecília Almadanim M, Pires IS, Abreu IA, Maroco J, Courtois B,
571 Gregorio GB, McNally KL, Margarida Oliveira M (2013) New allelic variants

- 572 found in key rice salt-tolerance genes: an association study. *Plant Biotech J* 11
573 (1):87-100
- 574 21. Ariyaratna HCK, Ul-Haq T, Colmer TD, Francki MG (2014) Characterization of
575 the multigene family TaHKT2;1 in bread wheat and the role of gene members in
576 plant Na⁺ and K⁺ status. *BMC Plant Biol* 14 (1):1
- 577 22. Mishra S, Singh B, Panda K, Singh BP, Singh N, Misra P, Rai V, Singh NK
578 (2016) Association of SNP haplotypes of HKT family genes with salt tolerance in
579 indian wild rice germplasm. *Rice* 9 (1):1
- 580 23. Kumar S, Beena A, Awana M, Singh A (2017) Physiological, biochemical,
581 epigenetic and molecular analyses of wheat (*Triticum aestivum*) genotypes with
582 contrasting salt tolerance. *Front Plant Sci* 8:1151
- 583 24. Diatloff E, Kumar R, Schachtman DP (1998) Site directed mutagenesis reduces
584 the Na⁺ affinity of HKT1, an Na⁺ energized high affinity K⁺ transporter. *FEBS*
585 *Lett* 432 (1-2):31-36
- 586 25. Böhm J, Scherzer S, Shabala S, Krol E, Neher E, Mueller T, Hedrich R (2016)
587 *Venus flytrap* HKT1-type channel provides for prey sodium uptake into
588 carnivorous plant without conflicting with electrical excitability. *Mol Plant* 9
589 (3):428-436
- 590 26. Almeida P, Katschnig D, de Boer AH (2013) HKT transporters-state of the art. *Int*
591 *J Mol Sci* 14 (10):20359-20385
- 592 27. Almeida P, de Boer G-J, de Boer AH (2014) Differences in shoot Na⁺
593 accumulation between two tomato species are due to differences in ion affinity of
594 HKT1;2. *J Plant Physiol* 171 (6):438-447
- 595 28. Ali A, Raddatz N, Aman R, Kim S, Park HC, Jan M, Baek D, Khan IU, Oh D-H,
596 Lee SY (2016) A single amino acid substitution in the sodium transporter HKT1
597 associated with plant salt tolerance. *Plant Physiol* 171: 2112–2126
- 598 29. Cao Y, Jin X, Huang H, Derebe MG, Levin EJ, Kabaleeswaran V, Pan Y, Punta
599 M, Love J, Weng J (2011) Crystal structure of a potassium ion transporter, TrkH.
600 *Nature* 471 (7338):336-340
- 601 30. Mian A, Oomen RJ, Isayenkov S, Sentenac H, Maathuis FJ, Véry AA (2011)
602 Over-expression of an Na⁺-and K⁺-permeable HKT transporter in barley improves
603 salt tolerance. *Plant J* 68 (3):468-479
- 604 31. Jabnoute M, Espeout S, Mieulet D, Fizames C, Verdeil J-L, Conéjéro G,
605 Rodríguez-Navarro A, Sentenac H, Guiderdoni E, Abdelly C (2009) Diversity in
606 expression patterns and functional properties in the rice HKT transporter family.
607 *Plant Physiol* 150 (4):1955-1971
- 608 32. Amar SB, Brini F, Sentenac H, Masmoudi K, Véry A-A (2014) Functional
609 characterization in *Xenopus* oocytes of Na⁺ transport systems from durum wheat
610 reveals diversity among two HKT1;4 transporters. *J Exp Bot* 65 (1):213-222
- 611 33. Munns R, James RA, Xu B, Athman A, Conn SJ, Jordans C, Byrt CS, Hare RA,
612 Tyerman SD, Tester M, Plett D, Gilliam M (2012) Wheat grain yield on saline
613 soils is improved by an ancestral Na⁺ transporter gene. *Nat Biotech* 30 (4):360-364
- 614 34. Byrt CS, Xu B, Krishnan M, Lightfoot DJ, Athman A, Jacobs AK, Watson-Haigh
615 NS, Plett D, Munns R, Tester M (2014) The Na⁺ transporter, TaHKT1;5-D, limits
616 shoot Na⁺ accumulation in bread wheat. *Plant J* 80 (3):516-526
- 617 35. Tounsi S, Amar SB, Masmoudi K, Sentenac H, Brini F, Véry A-A (2016)
618 Characterization of two HKT1;4 transporters from *Triticum monococcum* to
619 elucidate the determinants of the wheat salt tolerance *Nax1* QTL. *Plant Cell*
620 *Physiol* 57 (10):2047-2057
- 621

- 622 36. Baxter I, Brazelton JN, Yu D, Huang YS, Lahner B, Yakubova E, Li Y, Bergelson
623 J, Borevitz JO, Nordborg M (2010) A coastal cline in sodium accumulation in
624 *Arabidopsis thaliana* is driven by natural variation of the sodium transporter
625 *AtHKT1*; 1. PLoS Genet 6 (11):e1001193
- 626 37. Møller IS, Gilliam M, Jha D, Mayo GM, Roy SJ, Coates JC, Haseloff J, Tester
627 M (2009) Shoot Na⁺ exclusion and increased salinity tolerance engineered by cell
628 type-specific alteration of Na⁺ transport in *Arabidopsis*. Plant Cell 21 (7):2163-
629 2178
- 630 38. Plett D, Safwat G, Gilliam M, Møller IS, Roy S, Shirley N, Jacobs A, Johnson A,
631 Tester M (2010) Improved salinity tolerance of rice through cell type-specific
632 expression of *AtHKT1*; 1. PLoS One 5 (9):e12571
- 633 39. Munns R, Gilliam M (2015) Salinity tolerance of crops—what is the cost? New
634 Phytol 208 (3):668-673
- 635 40. Ismail AM, Horie T (2017) Genomics, physiology, and molecular breeding
636 approaches for improving salt tolerance. Annu Rev Plant Biol 68:405-434
- 637 41. Byrt CS, Platten JD, Spielmeyer W, James RA, Lagudah ES, Dennis ES, Tester
638 M, Munns R (2007) HKT1; 5-like cation transporters linked to Na⁺ exclusion loci
639 in wheat, *Nax2* and *Kna1*. Plant Physiol 143 (4):1918-1928
- 640 42. Vieira-Pires RS, Szollosi A, Morais-Cabral JH (2013) The structure of the KtrAB
641 potassium transporter. Nature 496 (7445):323-328
- 642 43. Fairbairn DJ, Liu W, Schachtman DP, Gomez-Gallego S, Day SR, Teasdale RD
643 (2000) Characterisation of two distinct HKT1-like potassium transporters from
644 *Eucalyptus camaldulensis*. Plant Mol Biol 43 (4):515-525
- 645 44. Liu W, Fairbairn DJ, Reid RJ, Schachtman DP (2001) Characterization of two
646 HKT1 homologues from *Eucalyptus camaldulensis* that display intrinsic
647 osmosensing capability. Plant Physiol 127 (1):283-294
- 648 45. Rodríguez-Navarro A, Ramos J (1984) Dual system for potassium transport in
649 *Saccharomyces cerevisiae*. J Bacteriol 159 (3):940-945
- 650 46. Laskowski RA, MacArthur MW, Moss DS, Thornton JM (1993) PROCHECK: a
651 program to check the stereochemical quality of protein structures. J Appl
652 Crystallogr 26 (2):283-291
- 653 47. Sippl MJ (1993) Recognition of errors in three-dimensional structures of proteins.
654 Proteins 17 (4):355-362
- 655 48. Gille C, Birgit W, Gille A (2013) Sequence alignment visualization in HTML5
656 without Java. Bioinformatics 30 (1):121-122
- 657 49. Edgar RC (2004) MUSCLE: multiple sequence alignment with high accuracy and
658 high throughput. Nucleic Acids Res 32 (5):1792-1797
- 659 50. Shen My, Sali A (2006) Statistical potential for assessment and prediction of
660 protein structures. Protein Sci 15 (11):2507-2524
- 661 51. Landau M, Mayrose I, Rosenberg Y, Glaser F, Martz E, Pupko T, Ben-Tal N
662 (2005) ConSurf 2005: the projection of evolutionary conservation scores of
663 residues on protein structures. Nucleic Acids Res 33 (suppl 2):W299-W302
- 664 52. Celniker G, Nimrod G, Ashkenazy H, Glaser F, Martz E, Mayrose I, Pupko T,
665 Ben-Tal N (2013) ConSurf: using evolutionary data to raise testable hypotheses
666 about protein function. Isr J Chem 53 (3-4):199-206
- 667 53. James RA, Blake C, Byrt CS, Munns R (2011) Major genes for Na⁺ exclusion,
668 *Nax1* and *Nax2* (wheat *HKT1;4* and *HKT1;5*), decrease Na⁺ accumulation in
669 bread wheat leaves under saline and waterlogged conditions. J Exp Bot 62
670 (8):2939-2947

- 671 54. Henderson SW, Gilliam M (2015) The “Gatekeeper” Concept: Cell-Type
672 Specific Molecular Mechanisms of Plant Adaptation to Abiotic Stress. In:
673 Molecular Mechanisms in Plant Adaptation. pp 83-115
674 55. Byrt CS (2008) PhD thesis: Genes for sodium exclusion in wheat. University of
675 Adelaide,
676 56. Kelley LA, Sternberg MJ (2009) Protein structure prediction on the Web: a case
677 study using the Phyre server. *Nat Protoc* 4 (3):363-371
678 57. Zhang Y (2008) I-TASSER server for protein 3D structure prediction. *BMC*
679 *Bioinformatics* 9 (1):1
680 58. Wu S, Zhang Y (2007) LOMETS: a local meta-threading-server for protein
681 structure prediction. *Nucleic Acids Res* 35 (10):3375-3382
682 59. Pei J, Kim BH, Grishin NV (2008) PROMALS3D: a tool for multiple protein
683 sequence and structure alignments. *Nucleic Acids Res* 36 (7):2295-2300
684 60. Sali A, Blundell T (1993) Comparative protein modelling by satisfaction of spatial
685 restraints. *J Mol Biol* 234 (3):779-815
686

1 **FIGURES AND FIGURE LEGENDS**

2

3 **Fig. 1 Mutation of G490R and K118E/L339P/Y379M in TmHKT1;5-A inhibited**

4 **its Na⁺ transport in heterologous expression systems. a.** Protein sequence

5 alignment of *HKT1;5* homologues from wheat, rice, barley, sorghum, *Medicago*

6 *truncatula* and Arabidopsis. The blue box indicates the 490 residue position of

7 TmHKT1;5-A and its homologues. The protein accession number are TmHKT1;5-A,

8 ABG33946.1; TaHKT1;5-B1, ABG33947.1; TaHKT1;5-B2, ABG33948.1;

9 TaHKT1;5-D, ABG33949.1; TtHKT1;5-B1, ABG33940.1; TtHKT1;5-B2,

10 ABG33941.1; HvHKT1;5, ABK58096.1; OsHKT1;5-Ni, Q0JNB6.1; OsHKT1;5-Po,

11 A2WNZ9.2; AtHKT1;1, Q84TI7.1; SbiHKT1;5, EES02856.1; MtHKT1;5,

12 AES77170.1; Tm, *Triticum monococcum*; Ta, *Triticum aestivum*; Tt, *Triticum*

13 *turgidum* subsp. *durum*; Hv, *Hordeum vulgare*; Os, *Oryza sativa*; At, *Arabidopsis*

14 *thaliana*; Sbi, *Sorghum bicolor*; Mt, *Medicago truncatula*. **b, c** Growth of *S.*

15 *cerevisiae* strain InvSc2 (MATa his-D1 leu2 trp1-289 ura3-52) expressing

16 *TmHKT1;5-A*, its two variants and empty-vector control on either the SC-Ura agar

17 medium (**b**) or the AP liquid medium (**c**). **b** A five serial dilutions of yeasts were

18 spotted on the SC-Ura medium with 2% (w/v) Gal, 1.67% (w/v) agar and indicated

19 Na level present and incubated at 30 °C for three days. **c** Optical density at 600 nm of

20 yeast growth in the liquid AP medium containing 0 mM or 10 mM NaCl. Data

21 represented in mean ± S.E.M, n = 3. **d-g** Heterologous expression of TmHKT1;5-A

22 and its two variants in *X. laevis* oocytes. **d** Confocal images of oocytes expressing

23 two variants tagged with *YFP* at the N-terminus. **e** Relative change in the ion profile

24 of oocytes expressing *TmHKT1;5-A* and its two variants to uninjected oocytes, data

25 represented in mean ± S.E.M, n = 3. **f** and **g** Current-voltage (I/V) curve of *X. laevis*

26 oocytes expressing *TmHKT1;5-A*, *TmHKT1;5-A*^{K118E/L339P/Y379M}, *TmHKT1;5-A*^{G490R}

27 and the H₂O-injected control. Oocytes expressing *TmHKT1;5-A* were recorded in 30

28 mM Na (**f**) and 10 mM K (**g**) glutamate; data represented in mean ± S.E.M, n = 5-9.

29

30 **Fig. 2 Molecular models of TmHKT1;5-A and G490R and K118E/L339P/Y379M**

31 **variants.** Cartoon representations of wild-type TmHKT1;5-A (**a**; cyan) and the

32 G490R (**b**; pink) and K118E/L339P/Y379M (**c**; orange) variants illustrate overall

33 folds in two orthogonal orientations (left and right panels). The left and right views in

34 panels **a-c** are related by 90° rotation about the horizontal axis. The structures of 3D
35 models are depicted in cartoon representations with cylindrical α -helices in wild-type
36 (**a**, G490 with the Van der Waals surface) or mutant (**b**, G490R with Van der Waals
37 surface; C, K118E, L339P, Y379M in atomic sticks) structures. Na⁺ ions are shown as
38 purple spheres located within the boundary of selectivity filters, where α -backbones
39 of pore-forming residues are coloured in red. Four substituted residues between wild-
40 type (**a**), and the G490R (**b**) and K118E/L339P/Y379M (**c**) variants are shown in
41 sticks and atomic colours. **d** A stereo view of four substitutions (G490R and
42 K118E/L339P/Y379M) shown on the opaque background of the cartoon structures
43 with Van der Waals surfaces in colours that are identical to those shown in panels (**a**-
44 **c**). Entries into the funnel of superposed transporters are indicated by a black arrows.
45

46 **Fig. 3 A stereo view of superposed TmHKT1;5-A and TaHKT1;5-D.** Six
47 differences in residues that are likely to underlie functional differences between the
48 proteins are depicted on the opaque background of cartoon structures with Van der
49 Waals surfaces. These residues are labelled by TmHKT1;5-A (first residue)
50 TaHKT1;5-D (last residue) numbering. The entries into the funnels of transporters are
51 indicated by black arrows.

52

53 **Fig. 4 Transport characteristics of TmHKT1;5-A, TmHKT1;5-A-D471 Δ , -D474G**
54 **and - D471 Δ /D474G in *X. laevis* oocytes. **a, b** The I/V curve (**a**) and transport**

55 conductance at -140 mV (**b**) of oocytes expressing *TmHKT1;5-A*, *TmHKT1;5-A^{D471 Δ}* ,
56 *TmHKT1;5-A^{D474G}* and *TmHKT1;5-A^{D471 Δ /D474G}* in 5 mM Na⁺ solution. **c** Na⁺-transport
57 affinity of TmHKT1;5-A, TmHKT1;5-A-D471 Δ , -D474G and - D471 Δ /D474G in *X.*
58 *laevis* oocytes. Michaelis-Menten kinetics of relative inward current at -140 mV, of
59 oocytes expressing *TmHKT1;5-A*, *TmHKT1;5-A^{D471 Δ}* , *TmHKT1;5-A^{D474G}* and
60 *TmHKT1;5-A^{D471 Δ /D474G}* in a serial Na⁺ solution of 0.01, 0.02, 0.05, 0.1, 0.5, 1, 2, 5, 10
61 and 30 mM. Data represent Mean \pm S.E.M, n = 6-9. Statistical difference was
62 determined by *Student's t*-test, asterick indicates statistical difference, **P* < 0.05.

63

64 **Fig. 5 Transport characteristics of TaHKT1;5-D, TaHKT1;5-D-D471⁺, -G473D**
65 **and -D471⁺/G473D in *X. laevis* oocytes. **a, b** The I/V curve (**a**) and transport**

66 conductance at -140 mV (**b**) of oocytes expressing *TaHKT1;5-D*, *TaHKT1;5-D^{D471⁺}*,
67 *TaHKT1;5-D^{G473D}* and *TaHKT1;5-D^{D471⁺/G473D}* in 5 mM Na⁺ solution. **c** Na⁺-transport

68 affinity of TaHKT1;5-D, TaHKT1;5-D-D471⁺, -G473D and -D471⁺/G473D in *X.*
69 *laevis* oocytes. Michaelis-Menten kinetics of relative inward current at -140 mV, of
70 oocytes expressing *TaHKT1;5-D*, *TaHKT1;5-D^{D471+}*, *TaHKT1;5-D^{G473D}* and
71 *TaHKT1;5-D^{D471+/G473D}* in a serial Na⁺ solution of 0.01, 0.02, 0.05, 0.1, 0.5, 1, 2, 5, 10
72 and 30 mM. Data represent Mean ± S.E.M, n = 5-6. Statistical difference was
73 determined by *Student's t*-test, astericks indicate statistical difference, **P* < 0.05 and
74 ***P* < 0.01.

75

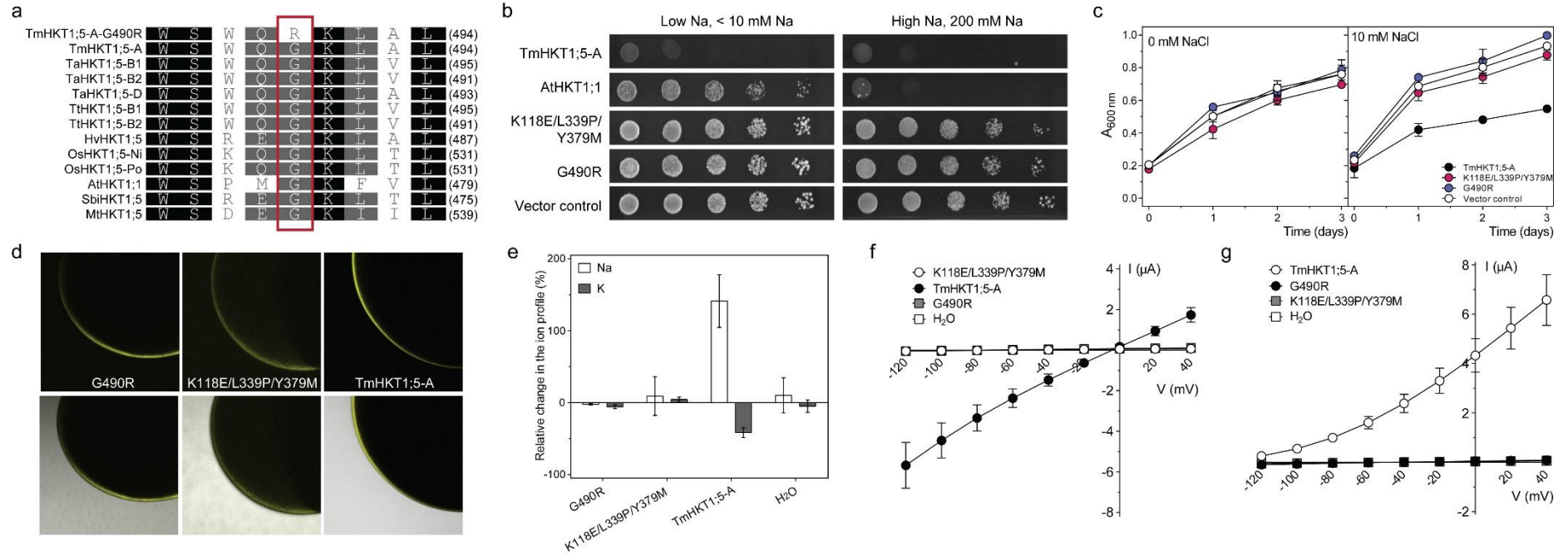
76 **Table 1.** A summary of differences in amino acid residues between TmHKT1;5-A
77 and TaHKT1;5-D that are likely significantly affect transport rates.

78

79

80

81 **Fig. 1**



82

83

Fig. 2

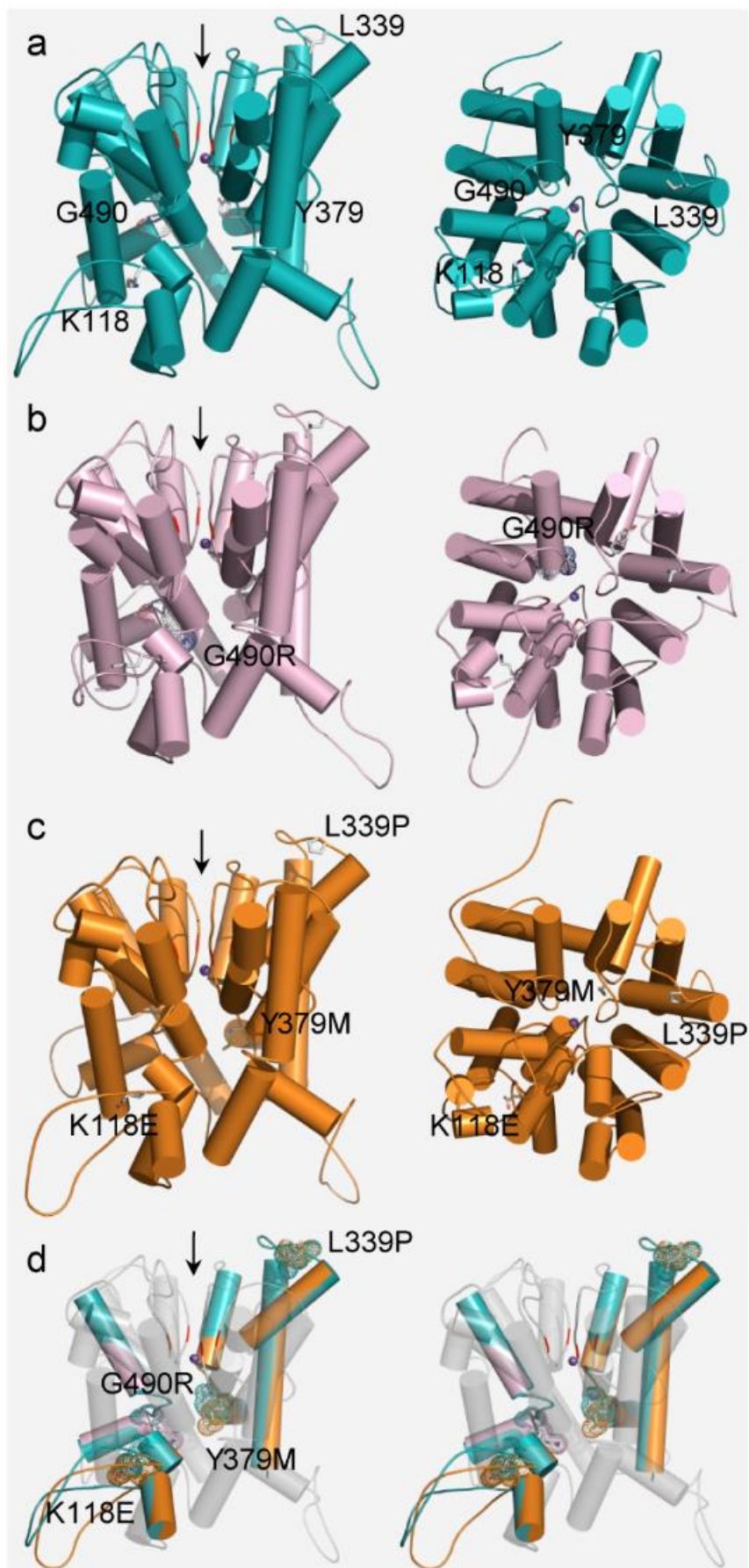


Fig. 3

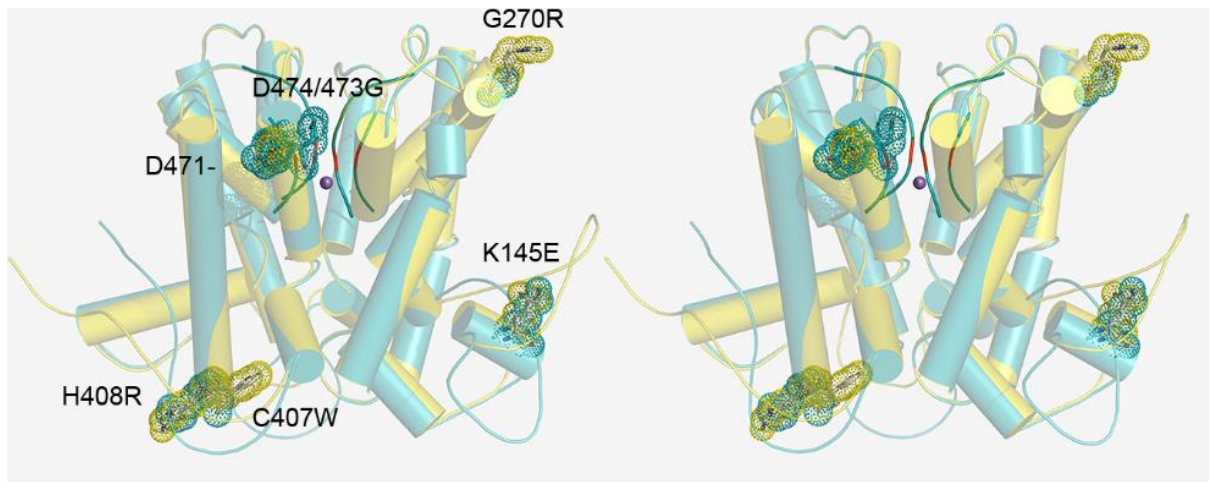


Fig. 4

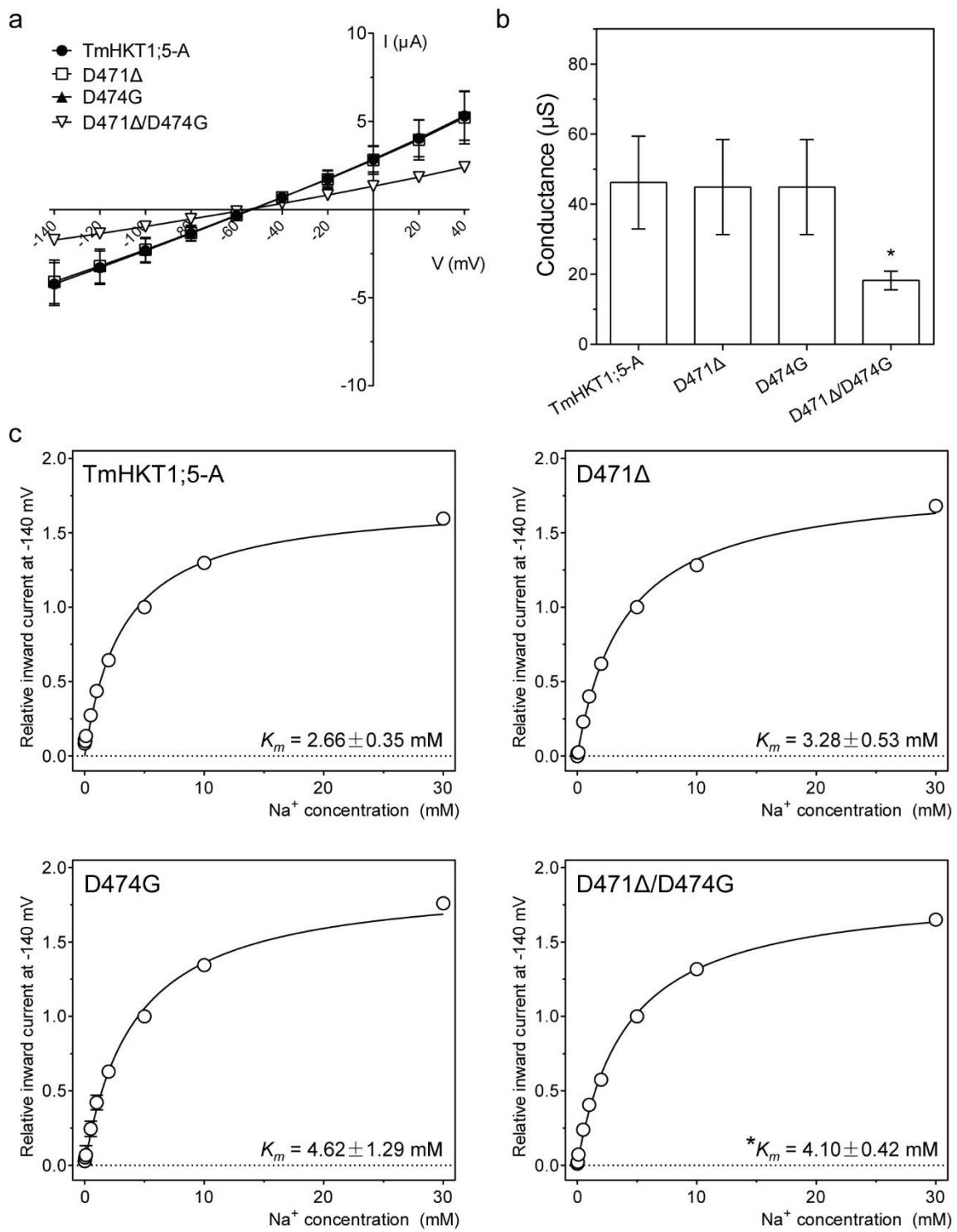


Fig. 5

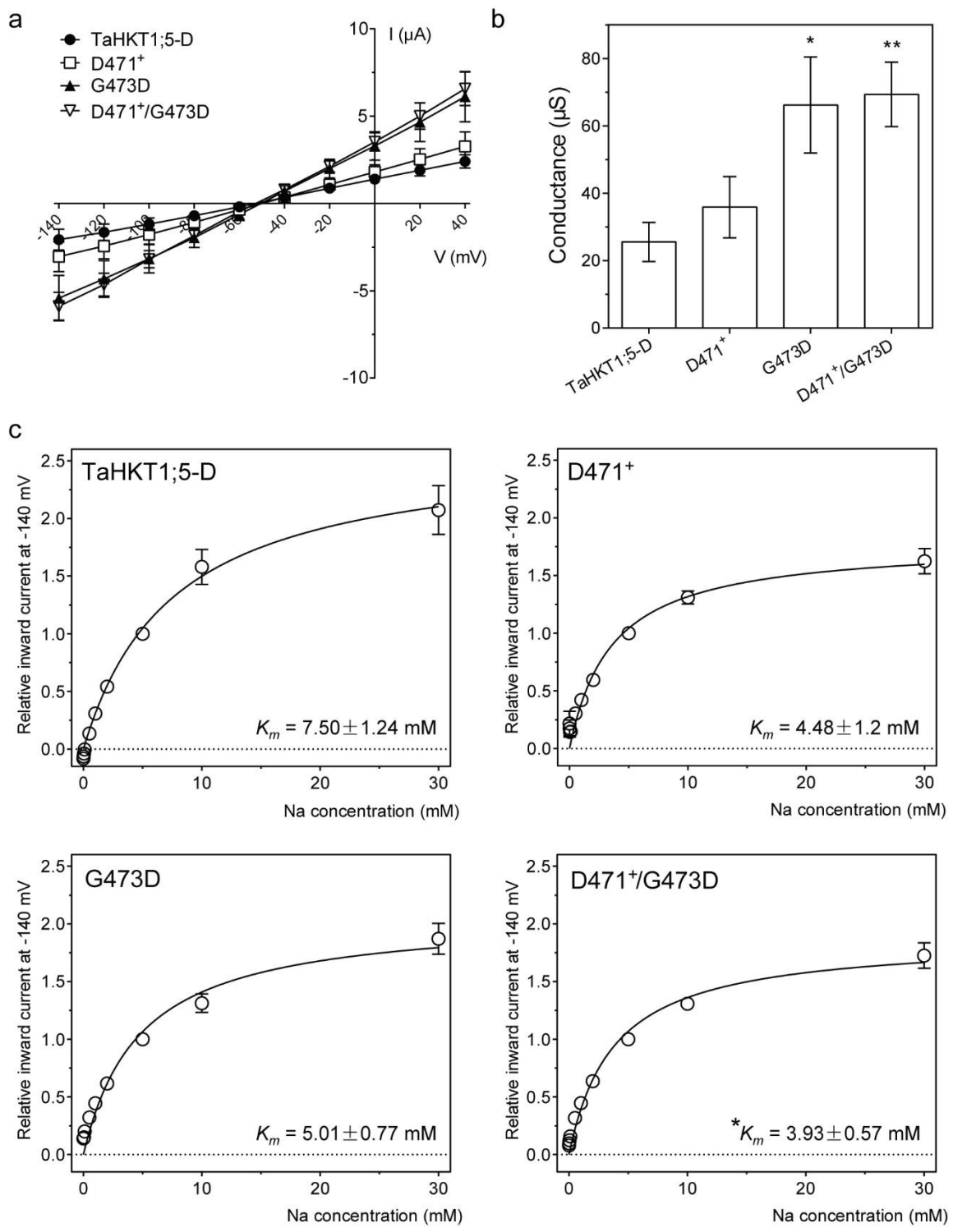


Table 1. A summary differences in amino acid residues between TmHKT1;5-A and TaHKT1;5-D that may significantly affect transport rates.

Residue number	Substitution		Predicted structural consequence of residue substitution or deletion
	TmHKT1;5-A	TaHKT1;5-D	
145	K	E	A change from a basic to an acidic residue. Likely to affect the local structure.
207	G	R	A substantial change in charge and volume of side chain. Expected to significantly alter the local structure.
407	C	W	Large difference in volume of a side chain at the base of an α -helix. Change in orientation of the α -helix.
408	H	R	Presence/ absence of the imidazole group from His. Significant change in the orientation of an α -helix, when combined with the C407W substitution.
471	D	-	Addition of an extra amino acid residue. Significant impact on a local structure.
474/473	D	G	Large charge difference combined with change of the volume of the side chain. Effect on packing of the structure, when combined with the nearby D471- substitution.